Proc. Natl. Acad. Sci. USA
Vol. 91, pp. 10670–10674, October 1994
Biophysics

Proofreading DNA: Recognition of aberrant DNA termini by the Klenow fragment of DNA polymerase I

(polymerase and 3′-5′ exonuclease sites/DNA partitioning/mismatched base pairs/time-resolved fluorescence spectroscopy)

THEODORE E. CARVER, JR., REMO A. HOCHSTRASSER†, AND DAVID P. MILLAR‡

Department of Molecular Biology, The Scripps Research Institute, La Jolla, CA 92037

Communicated by Bruno H. Zimm, June 14, 1994 (received for review September 22, 1993)

ABSTRACT **Fluorescence depolarization decays were measured for 5-dimethylaminonaphthalene-1-sulfonyl (dansyl) probes attached internally to 17-mer·27-mer oligonucleotides bound to Klenow fragment of DNA polymerase I. The time-resolved motions of the dansyl probes were sensitive indicators of DNA–protein contacts, showing that the protein binds to DNA with two footprints, corresponding to primer termini at either the polymerase or 3′-5′ exonuclease sites. We examined complexes of Klenow fragment with DNAs containing various base mismatches. Single mismatches at the primer terminus caused a 3- to 4-fold increase in the equilibrium partitioning of DNA into the exonuclease site; the largest effects were observed for purine–purine mismatches. Two or more consecutive G·G mismatches caused the DNA to bind exclusively at the exonuclease site, with a partitioning constant at least 250-fold greater than that of the corresponding matched DNA sequence. Internal single mismatches produced larger effects than the same mismatch at the primer terminus, with a $\Delta\Delta G$ relative to the matched sequence of −1.1 to −1.3 kcal/mol for mismatches located 2, 3, or 4 bases from the primer terminus. Although part of the observed effects may be attributed to the increased melting capacity of the DNA, it appears that the polymerase site also promotes movement of DNA into the exonuclease site by rejecting aberrant primer termini. These effects suggest that the polymerase and exonuclease sites act together to recognize specific errors that distort the primer terminus, such as frameshifts, in addition to proofreading misincorporated bases.**

A necessary feature of all DNA-dependent DNA polymerases is the ability to copy DNA with high fidelity; for DNA polymerase I, the probability of an error during replication is $\leq 10^{-6}$ per nt addition (1). Exonucleolytic proofreading contributes to replication fidelity through the preferential excision of mismatched bases after mispair synthesis occurs (for reviews, see refs. 2–4). In DNA polymerase I, proofreading is accomplished by a 3′-5′ exonuclease in a separate domain of the same polypeptide with 5′-3′ polymerase activity.

The crystal structure of the 70-kDa Klenow fragment of DNA polymerase I has been determined. Klenow fragment consists of two putative DNA-binding clefts divided by a "thumb-like" domain (5). The 5′-3′ polymerase and 3′-5′ exonuclease activities are separated by 30–40 Å, indicating that shuttling of the DNA between the two sites is a requirement for proofreading. Joyce and Steitz (6) have proposed a structural model for movement of DNA from the polymerase site to the exonuclease site. In this model, 3- to 4-bp melt at the primer terminus, followed by movement of the resulting single-stranded region of DNA into the exonuclease site (7). From assays using biotinylated DNA substrates, there is evidence that the polymerase–exonuclease transition involves an 8-bp translocation of the protein upstream on the DNA (8). However, a recent structure of duplex DNA bound to Klenow fragment shows the primer terminus bound in the cleft adjacent to the exonuclease site, much closer to both active sites than thought (9). Currently, the mechanism of DNA movement within the protein remains unclear. In addition, the effects of protein and DNA structure upon the binding of DNA to each site have not been resolved.

The kinetics of misincorporation and proofreading in the Klenow fragment have been examined in detail using quenched-flow techniques, and the scheme required to describe interconversion of the intermediate states is complex (10, 11). For a simple model in which only DNA binding is considered, preferential excision of mismatched bases is achieved by increasing the rate of exonucleolysis of the terminal nucleotide relative to the rate of addition of the next nucleotide. An increase in the ratio of exonuclease to polymerase rates could be due to a decrease in the intrinsic rate of polymerization, k_{pol}, or to an increase in the partitioning of DNA from the polymerase site into the exonuclease site, or to a combination of these effects (Fig. 1). The greater melting capacity of mispaired termini could contribute to increased partitioning of DNA into the exonuclease site (12). In addition, it is important to note that any structural feature of the DNA favoring DNA binding at the exonuclease site over binding at the polymerase site will increase the rate of exonucleolysis relative to polymerization. Because movement of DNA between the polymerase and exonuclease sites appears markedly faster than the intrinsic rates of the reactions occurring at either site, the partitioning step is at equilibrium relative to the other processes and can be represented by the equilibrium constant for partitioning of DNA termini between the polymerase and exonuclease sites, K_{pe} (Fig. 1).

In this study, we examine the effects of base mismatches and sequence variation upon binding of DNA to the polymerase and exonuclease sites of Klenow fragment. The time-resolved fluorescence depolarization of a 5-dimethylaminonaphthalene-1-sulfonyl (dansyl) probe covalently attached to DNA contains information about partitioning of the DNA between the polymerase and 3′-5′ exonuclease sites of the enzyme (13). This technique is used here to estimate the internal partitioning constant K_{pe} for a series of defined oligonucleotide primer/templates containing either matched or mismatched sequences.

EXPERIMENTAL METHODS

Materials. The exonuclease-deficient D424A mutant of Klenow fragment was purified from *Escherichia coli* CJ376,

The publication costs of this article were defrayed in part by page charge payment. This article must therefore be hereby marked "*advertisement*" in accordance with 18 U.S.C. §1734 solely to indicate this fact.

Abbreviations: dansyl, 5-dimethylaminonaphthalene-1-sulfonyl; K_{pe}, equilibrium constant for partitioning of DNA termini between the polymerase and exonuclease sites.

†Present address: Biophysikalische Chemie, Biozentrum, CH-4056 Basel, Switzerland.
‡To whom reprint requests should be addressed.

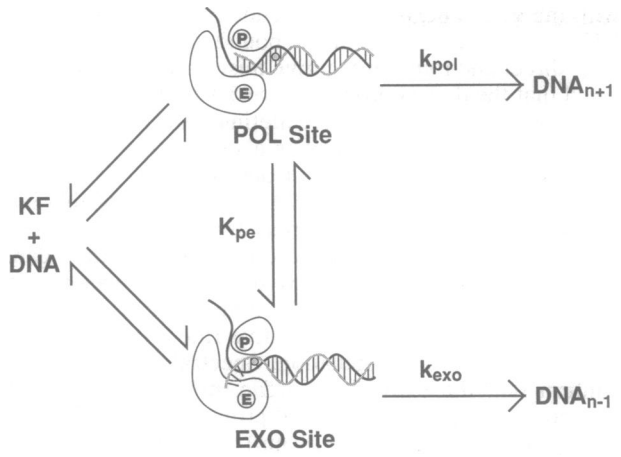

FIG. 1. Simplified scheme for a single round of DNA processing by Klenow fragment of DNA polymerase I. k_{pol} is the intrinsic rate constant for addition of the next nucleotide to DNA bound at the polymerase site, and k_{exo} is the intrinsic rate constant for exonucleolysis of DNA bound at the exonuclease site. The active sites for the polymerization reaction and the 3′-5′ exonuclease reaction are denoted P and E, respectively. The DNA primer and template strands are shown as stippled and solid lines, respectively. The circle located within the DNA helix represents an internal dansyl probe attached via a 3-carbon linker to a uridine base 7 bp from the primer terminus. When DNA termini are bound to the polymerase site, the dansyl probe is exposed to solvent. Movement of the DNA terminus into the exonuclease site shifts the footprint of the protein, drawing the probe into the protein interior. The different footprints for polymerase- and exonuclease-bound DNA could result from either a translocation of the DNA or a conformational shift in the enzyme that exposes different faces of the DNA helix to solvent. The 3′ terminal region of the primer strand may be single-stranded within the exonuclease site. Note that the polymerase and exonuclease reactions are inhibited during the present equilibrium partitioning measurements.

as described (14). The *E. coli* CJ376 cells were provided by C. Joyce (Yale University). Protein samples were found to be >95% pure by PAGE. Dansyl-labeled oligonucleotide 17-mers were synthesized, derivatized, and purified by HPLC as described (15). Before each measurement, 10 μM labeled 17-mer and 11 μM 27-mer were mixed and annealed at 75°C for 10 min. Klenow fragment was then added to a final concentration of 12 μM. The conditions for all fluorescence experiments were 50 mM Tris, pH 7.5/3 mM $MgCl_2$, 20°C.

The dansyl probe does not significantly perturb the binding of DNA to Klenow fragment (16). For each protein–DNA complex, we established using a steady-state fluorescence titration that equimolar amounts of protein and DNA resulted in a saturated complex.

Time-Resolved Fluorescence Spectroscopy. The experimental setup for the collection of isotropic fluorescence and polarization anisotropy decay data has been described (13). Samples were excited with the frequency-doubled output of a synchronously mode-locked and cavity-dumped CW Radiation dye laser at 318 nm. Fluorescence emissions were passed through a WG335 filter (Schott, Mainz, F.R.G.) and a single-grating monochromator, and all measurements were made at an emission wavelength of 535 nm using a microchannel plate photomultiplier and time-correlated single photon-counting detection system (13). Decays were measured in 512 channels with a time resolution of 88 ps per channel.

Data Analysis. The fluorescence anisotropy at time t is computed from polarized components of the time-resolved fluorescence as

$$r(t) = [I_{\parallel}(t) - I_{\perp}(t)]/[I_{\parallel}(t) + 2I_{\perp}(t)], \quad [1]$$

where $I_{\parallel}(t)$ and $I_{\perp}(t)$ are the observed intensity decays when the observing polarizer is oriented parallel (∥) or perpendicular (⊥) to the direction of the vertically polarized exciting light. For a homogeneous population of dansyl probes attached to DNA, the contributions made by various types of motion to the time-dependent fluorescence anisotropy $r(t)$ can be represented as

$$r(t) = \beta_1 \exp(-t/\phi_1) + \beta_2 \exp(-t/\phi_2), \quad [2]$$

where ϕ_1 is the correlation time for local rotation of the probe (1 − 2 ns), and ϕ_2 is the correlation time for overall tumbling of the DNA–protein complex (≈60 ns). β_1 and β_2 are the corresponding anisotropy amplitudes for the two components. If the probe population is heterogeneous, each subpopulation of probes will have its own associated amplitudes and decay times. For a two-state model, in which one state corresponds to probe molecules that are largely exposed to solvent, whereas the other state corresponds to probes that are buried within the protein, the time-dependent anisotropy is

$$r(t) = f_e(t)r_e(t) + f_b(t)r_b(t), \quad [3]$$

where $f_e(t)$ is the fraction of fluorescence at time t due to the exposed probes, $r_e(t)$ describes the anisotropy decay of the exposed probes, and $f_b(t)$, $r_b(t)$ are the corresponding quantities for the buried probes (17). The fractions $f_e(t)$ and $f_b(t)$ are complex functions of the fluorescence lifetimes of the exposed and buried probes (13):

$$f_e(t) = \frac{x_e \sum_{j=1}^{N} \alpha_{je} \exp(-t/\tau_{je})}{x_e \sum_{j=1}^{N} \alpha_{je} \exp(-t/\tau_{je}) + x_b \sum_{j=1}^{M} \alpha_{jb} \exp(-t/\tau_{jb})}, \quad [4]$$

where τ_{jb}, α_{jb}, and τ_{je}, α_{je} are the corresponding lifetimes and amplitudes for the two populations. An analogous expression was used for $f_b(t)$. Immediately after excitation ($t = 0$), $f_e(t)$ and $f_b(t)$ are the actual fractions of exposed and buried probes, x_e and x_b, respectively, assuming that the extinction coefficient and radiative rate constant are the same for both populations. At longer times in the decay, $f_b(t)$ becomes larger than $f_e(t)$, due to the longer lifetimes of the buried probes relative to the exposed probes. These conditions can cause a "dip and rise" in the observed anisotropy decay, which facilitates the measurement of very small amounts of buried probes (Fig. 2, ref. 13).

The fractions of buried dansyl probes in each experiment, corresponding to the fraction of DNA termini bound at the exonuclease site, were obtained from a global fit of all the anisotropy decay data to Eq. 3 using nonlinear least-squares methods (18). Intensity decay curves were not deconvolved because the response of the detection system 45 ps (full width at half-maximum) was essentially instantaneous on the time scale of the measurements (45-ns full scale). The anisotropy data were assigned appropriate weighting factors in the fit (19). The amplitudes and decay times describing each $f(t)$ and $r(t)$ population were optimized for best fit but were linked for all the data sets, whereas x_b was optimized independently for each data set.

RESULTS

Fluorescence and Anisotropy Decays of Dansyl Probes. Previous studies of a dansyl probe attached to free duplex DNA indicate that the dansyl moiety is probably located in the major groove of the DNA helix in a flexible conformation (13). Time-resolved fluorescence measurements made upon

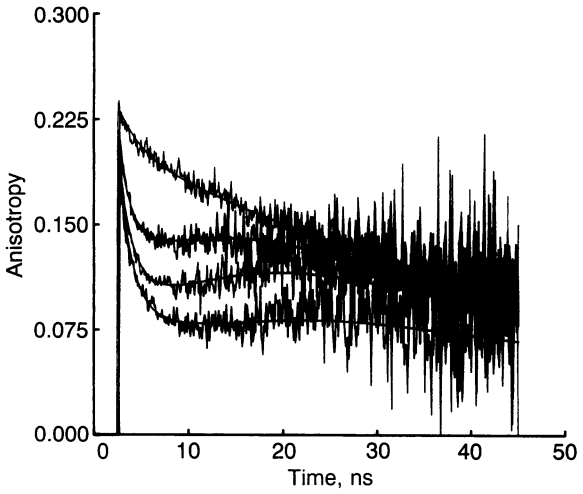

FIG. 2. Time courses for polarization anisotropy decays of D424A Klenow fragment–DNA complexes in 50 mM Tris·HCl, pH 7.5 at 20°C. The duplex DNAs used in each experiment were, from the top curve to the bottom curve: 17*G·27-3G1A, four consecutive purine–purine mismatches at the primer terminus; 17*G·27-A+3, an A·A mismatch four bases from the terminus; 17*G·27-G, a single G·G mismatch at the end of the primer strand; and 17*G·27-C, a matched DNA terminus. The fitted curves (solid lines) were obtained from a global fit of 16 data sets to a two-state model (Eq. 3). The parameters describing the fluorescence and anisotropy decays for exposed and buried probes were linked for all data sets. Two lifetimes ($M = 2$) were sufficient to represent the fluorescence decay of the buried probes, whereas three lifetimes ($N = 3$) were required for the exposed probes. The fitted values of the linked lifetime and anisotropy parameters were $\tau_{1e} = 1.01$ ns, $\tau_{2e} = 4.13$ ns, $\tau_{3e} = 11.9$ ns, $\alpha_{1e} = 0.30$, $\alpha_{2e} = 0.674$, $\alpha_{3e} = 0.026$, $\phi_{1e} = 1.24$ ns, $\phi_{2e} = 57.2$ ns, $\beta_{1e} = 0.11$, $\beta_{2e} = 0.081$, $\tau_{1b} = 3.06$ ns, $\tau_{2b} = 18.4$ ns, $\alpha_{1b} = 0.70$, $\alpha_{2b} = 0.30$, $\phi_{1b} = 1.24$ ns, $\phi_{2b} = 57.2$ ns, $\beta_{1b} = 0.028$, $\beta_{2b} = 0.208$. The fitted fraction of buried dansyl probes, equivalent to the fraction of exonuclease-bound DNA, and the reduced χ^2 recovered for each data set were, from top to bottom: $x_b = 0.96$, $\chi_r^2 = 1.14$; $x_b = 0.41$, $\chi_r^2 = 1.26$; $x_b = 0.18$, $\chi_r^2 = 1.18$; and $x_b = 0.042$, $\chi_r^2 = 1.22$.

the free duplex DNAs (sequences shown in Table 1) revealed that the probes have three fluorescence lifetimes that are independent of the sequence of the last six bases at the 3′ end of the primer strand; the anisotropy decays were also identical for all of the free duplexes we examined. These results indicate that in the absence of Klenow fragment, changing the terminus sequence does not affect the environment of the upstream dansyl probe.

Fluorescence anisotropy decays measured for DNAs bound to Klenow fragment revealed a striking effect of the terminus sequence (Fig. 2). The differences observed in the anisotropy decays indicate that the probe environment was different in each DNA–protein complex. Similar anisotropy decays were observed when the DNAs were added to D424A Klenow fragment that had been preincubated in 50 mM EDTA, showing that the observed effects were not caused by partial exonucleolytic degradation of the DNA because exonucleolysis was inhibited in the absence of divalent cations. To determine if the observed differences in the probe environment for each DNA–protein complex could be resolved by a two-state model, we globally fitted 16 time-resolved anisotropy decays using Eqs. 3 and 4 (Fig. 2, Table 1). The global reduced χ^2 (χ_r^2) for this fit was 1.150, and the local χ_r^2 for all the data sets were in the range 0.99–1.3. The good quality of the global fit demonstrates that the heterogeneous probe populations could be modeled adequately by two states, a solvent-exposed state permitting extensive local motion and a protein-associated state with restricted local motion of the dansyl probes (Fig. 2). Furthermore, the fitted parameters for exposed probes in the global analysis agreed with the values measured independently for the free duplex DNAs. For Klenow fragment bound to DNAs containing two, three, and four consecutive mismatches, our data indicated that the dansyl probes are >95% in the protein-buried state. The independently fitted lifetime and anisotropy decay parameters for these complexes also agreed with those recovered for the buried probes from the global fit.

Because the two protein–DNA complexes probably interconvert in milliseconds, whereas the dansyl fluorescence emission is complete in nanoseconds, the fraction of dansyl probes in each environment, x_b or x_e, is equivalent to the fraction of DNA bound in each complex, provided that the extinction coefficients and radiative rate constants are the same for each probe population. Spectral data (not shown) confirm that the extinction coefficients and radiative rate constants of exposed and buried probes do not differ significantly at the excitation (318 nm) and emission (535 nm) wavelengths, respectively. In previous fluorescence anisotropy decay experiments, the buried probe population was assigned to DNA termini bound at the exonuclease site of Klenow fragment (13). This assignment was confirmed here by the observation that the anisotropy decay of Klenow fragment bound to DNA containing two or more consecutive mispairs reveals a homogeneous population of fully buried probes. Therefore, the partitioning constant for DNA binding to the exonuclease site was calculated from the measured fraction of buried probes, $K_{pe} = x_b/(1 - x_b)$.

Table 1 reports K_{pe} values for 14 primer/template sequences. The base sequence in a 4-base region between the primer terminus and the dansyl probe was systematically varied in this series, whereas the remainder of the base sequence was common to each DNA (Table 1). The sequences were designed so that the effect of single mismatched base pairs on partitioning of DNA could be examined, as well as the effects of mismatch position and multiple consecutive mismatches. Most of the DNAs contained a constant primer sequence (denoted 17*G) and either a matched or mismatched template sequence. A second primer sequence (17*TG) was used in some of the measurements to assess the effect of the flanking sequence on partitioning of the primer terminus between active sites. Two of the DNAs also contained a 10-mer oligonucleotide annealed to the 5′ region of the template strand, so that partitioning could be compared in the presence or absence of a single-stranded template overhang.

We note that as x_b becomes large, the value of K_{pe} becomes poorly defined, and any measured fraction >0.95 was reported as a $K_{pe} \geq 19$ (Table 1). The free energy of partitioning discrimination, $\Delta\Delta G_{pe}$, was computed as $-RT \ln(K_{pe}/K_{matched})$, where K_{pe} is the partitioning constant for a particular mismatched sequence and $K_{matched}$ is the partitioning constant for the corresponding matched sequence.

Effects of Terminus Sequence. The equilibrium constants for partitioning two matched DNA duplexes into the exonuclease site are presented in Table 1. The two primer sequences contain either a (G+C)-rich sequence (17*G) or an (A+T)-rich sequence (17*TG) adjacent to the primer 3′ terminus. We could resolve very small differences in the abundance of each form of the different DNA–protein complexes, due to the large contribution of buried probes at longer times in the anisotropy decay (Fig. 2). The partitioning constant was roughly 2-fold larger for the matched duplex containing the terminal primer sequence AATG than for the duplex containing the terminal sequence AGGG (Table 1).

Effects of Single Mismatches. Partitioning of duplexes containing terminal G·G, G·A, and G·T mismatches was measured for the 17*G primer and for the G·G mismatch in the 17*TG primer (Table 1). We found that single mismatches increased K_{pe} ≈3-fold, with the G·T mismatch producing slightly smaller effects than the purine–purine mismatches.

Table 1. Partitioning constants for DNA binding to the exonuclease and polymerase domains of Klenow fragment

Oligonucleotide	DNA sequence	K_{pe}	$\Delta\Delta G_{pe}$, kcal/mol
	Matched sequences		
17*G·27-C	5′-TCGCAGCCGUCCAAGGG 3′-AGCGTCGGCAGGTTCCCATATAGCCGA	0.070 ± 0.02†	0
17*TG·27B-C	5′-TCGCAGCCGUCAAAATG 3′-AGCGTCGGCAGTTTTACATATAGCCGA	0.16	0
	Single mismatches		
17*G·27-T	5′-TCGCAGCCGUCCAAGGG 3′-AGCGTCGGCAGGTTCCTATATAGCCGA	0.18	−0.53
17*G·27-A	5′-TCGCAGCCGUCCAAGGG 3′-AGCGTCGGCAGGTTCCAATATAGCCGA	0.22	−0.66
17*G·27-G	5′-TCGCAGCCGUCCAAGGG 3′-AGCGTCGGCAGGTTCCGATATAGCCGA	0.22	−0.66
17*TG·27B-G	5′-TCGCAGCCGUCAAAATG 3′-AGCGTCGGCAGTTTTAGATATAGCCGA	0.59	−0.78
	Multiple consecutive mismatches		
17*G·27-G	5′-TCGCAGCCGUCCAAGGG 3′-AGCGTCGGCAGGTTCCGATATAGCCGA	0.22	−0.66
17*G·27-2G	5′-TCGCAGCCGUCCAAGGG 3′-AGCGTCGGCAGGTTCGGATATAGCCGA	≥19‡	≤−3.3
17*G·27-3G	5′-TCGCAGCCGUCCAAGGG 3′-AGCGTCGGCAGGTTGGGATATAGCCGA	≥19‡	≤−3.3
17*G·27-3G1A	5′-TCGCAGCCGUCCAAGGG 3′-AGCGTCGGCAGGTAGGGATATAGCCGA	≥19‡	≤−3.3
	Internal mismatches		
17*G·27-G	5′-TCGCAGCCGUCCAAGGG 3′-AGCGTCGGCAGGTTCCGATATAGCCGA	0.22	−0.66
17*G·27-G+1	5′-TCGCAGCCGUCCAAGGG 3′-AGCGTCGGCAGGTTCGCATATAGCCGA	0.63	−1.3
17*G·27-G+2	5′-TCGCAGCCGUCCAAGGG 3′-AGCGTCGGCAGGTTGCCATATAGCCGA	0.46	−1.1
17*G·27-A+3	5′-TCGCAGCCGUCCAAGGG 3′-AGCGTCGGCAGGTACCCATATAGCCGA	0.70	−1.3
17*G·27-G+1:10M	5′-TCGCAGCCGUCCAAGGG/TATATCGGCA 3′-AGCGTCGGCAGGTTCGC-ATATAGCCGA	0.33	−0.9
17*G·27-A+3:10M	5′-TCGCAGCCGUCCAAGGG/TATATCGGCT 3′-AGCGTCGGCAGGTACCC-ATATAGCCGA	0.58	−1.2

U denotes the modified uridine base linked to a dansyl probe. Mismatched base pairs are underlined. Errors in K_{pe} were ≈±15%, with the exceptions noted below.

†The error estimate for this value is the SD of three independent determinations.

‡These values are lower limits for the value of K_{pe}, because the error of measurement prevented accurate estimates of fractions of binding >0.95.

The G·T mispair is formed most frequently in primer extension experiments with Klenow fragment (20). For the (A+T)-rich sequence containing a terminal G·G mismatch, K_{pe} was >2-fold larger than for the (G+C)-rich sequence containing the same terminal mismatch. However, the relative values for partitioning of mismatched versus matched DNA, reflected in $\Delta\Delta G_{pe}$, were similar for both sequences (Table 1).

Effects of Consecutive and Internal Mismatches. The polarization anisotropy decays for DNAs containing two or more consecutive mismatches indicated a homogenous population of DNA molecules that were completely bound at the exonuclease site. The identical limiting values obtained for two, three, and four mismatches, coupled with the homogeneity of the probe populations, indicates that essentially 100% of the DNA is bound at the exonuclease site when multiple G·G mismatches are present at the primer terminus. The shift to the exonuclease site caused by multiple mismatches represents at least a 250-fold increase in the equilibrium constant for partitioning into the exonuclease domain relative to the matched sequence (Table 1). Because K_{pe} was calculated from the fractional amount of DNA bound at the exonuclease site, the K_{pe} values reported for two, three, and four mismatches probably underestimate the true partitioning constant, and we reported these as minimum values.

Large effects were also observed for single mismatches located at various positions upstream of the primer terminus. An internal G·G mismatch at any of these interior positions resulted in larger K_{pe} values than observed for a G·G mismatch at the primer terminus (Table 1).

DISCUSSION

Preferential partitioning of mismatched DNA termini from the polymerase to exonuclease sites of Klenow fragment could result from an increased melting capacity of the primer terminus or from weaker binding of the DNA at the polymerase site. The intrinsic affinity of DNA for the exonuclease site is directly related to melting capacity because the 3′-5′

exonuclease of Klenow fragment strongly prefers a single-stranded substrate (7, 21). We found that the matched (A+T)-rich terminus showed greater partitioning into the exonuclease site compared with a matched (G+C)-rich terminus, demonstrating that binding to the exonuclease domain is favored by sequences that promote increased melting of the primer terminus. This result is consistent with the greater rate of exonucleolysis seen for (A+T)-rich sequences compared with (G+C)-rich sequences (22). In addition to increasing the melting capacity of the primer terminus, homopolymeric A/T runs promote primer-template slippage under certain conditions and may have an altered DNA conformation at the primer terminus that inhibits DNA binding at the polymerase site (23, 24).

The presence of a single mismatch at the terminal base pair of the DNA substrate promotes binding of DNA to the exonuclease site; average free energy difference is −0.6 to −0.7 kcal/mol. This increase is significantly larger than can be accounted for solely in terms of greater melting capacity of the primer terminus. Petruska, Goodman, and coworkers (25) measured $\Delta\Delta S°$ and $\Delta\Delta H°$ for melting a 9-bp DNA duplex containing a terminal G·T mismatch with the sequence -ATGGG at the 3′ terminus. This sequence is very similar to the terminal sequence of 17*G·27-T (-AAGGG, Table 1). Melting data for the 9-mer duplex (25) yield an estimate of ≈−0.2 kcal/mol for the contribution of a terminal G·T mismatch to the free energy of melting of the DNA at 20°C. This value is a factor of three smaller than the free energy of partitioning that we observed for the 17*G·27-T sequence (Table 1). The difference between the melting and partitioning free energies indicates that both weaker DNA binding at the polymerase site and greater melting capacity of the primer terminus contribute to partitioning of mismatched primer termini into the exonuclease site of Klenow fragment. Furthermore, the large increase in partitioning into the exonuclease site observed for two or more consecutive terminal mismatches, together with the observed effects of the flanking sequence on partitioning of the terminus, suggest that melting of at least two terminal base pairs is required to transfer the primer terminus from the polymerase site to the exonuclease site. Thus, our data are consistent with the "slide and melt" model of proofreading in DNA polymerase I (6), with evidence that the enzyme can promote melting of the DNA terminus.

When single G·G mismatches were placed upstream from the DNA terminus, the free energy of discrimination relative to a matched base pair was in the range −1.1 to −1.3 kcal/mol (Table 1). This effect persisted for single mismatches up to 4 bp from the primer terminus. An internal mismatch may produce a local structural distortion, or bulge, in the double helix that inhibits binding in the polymerase domain. *Drosophila* DNA polymerase α holoenzyme, which lacks a 3′-5′ exonuclease activity, is inhibited by mismatches several bases upstream from the primer terminus, and this effect was attributed to a reduced affinity of the protein for DNA containing internal mismatches (26).

The preferential partitioning of DNA containing multiple and internal mismatches into the exonuclease site suggests that the exonuclease and polymerase sites may act together to recognize mutagenic errors, such as frameshift errors, that distort the DNA upstream from the primer terminus. The exonuclease domain could assist in the correction of these errors both by exonucleolytic cleavage and by simple melting and realignment of the DNA terminus after partitioning into the exonuclease domain. The latter mechanism does not require exonuclease activity to increase fidelity. Such a mechanism is supported by fidelity studies with various Klenow fragment derivatives, in which a derivative containing a catalytically inactive exonuclease domain exhibited fewer frameshift errors than a derivative lacking the exonuclease domain entirely (1). Klenow fragment also has 10- to 40-fold higher frameshift fidelity than several other DNA polymerases lacking an exonuclease domain (1, 27).

The partitioning constants for the 17*G·27-A+3·10M and 17*G·27G+1·10M duplexes, in which the 5′ overhang of the 27-mer template was annealed with a 10-mer to form a duplex, show that DNA polymerase I can recognize a deformed terminus lacking a single-stranded 5′-template overhang (Table 1). These data indicate that exonucleolytic proofreading can occur on a nicked DNA duplex, after a single-stranded gap has been filled by the polymerase activity.

We thank Dwayne Allen for advice on synthesis of dansyl-labeled DNA. This research was supported by National Institutes of Health Grant GM44060 (D.P.M.) and National Research Service Award Postdoctoral Fellowship GM15729 (T.E.C.). R.A.H. gratefully acknowledges support from the Swiss National Science Foundation.

1. Bebenek, K., Joyce, C. M., Fitzgerald, M. P. & Kunkel, T. A. (1990) *J. Biol. Chem.* **265,** 13878–13887.
2. Goodman, M. F., Creighton, S., Bloom, L. B. & Petruska, J. (1993) *Crit. Rev. Biochem. Mol. Biol.* **28,** 83–126.
3. Carroll, S. S. & Benkovic, S. J. (1990) *Chem. Rev.* **90,** 1291–1307.
4. Echols, H. & Goodman, M. F. (1991) *Annu. Rev. Biochem.* **60,** 477–511.
5. Ollis, D. L., Brick, P., Hamlin, R., Xuong, N. G. & Steitz, T. A. (1985) *Nature (London)* **313,** 762–766.
6. Joyce, C. M. & Steitz, T. A. (1987) *Trends Biochem. Sci.* **12,** 288–292.
7. Freemont, P. S., Friedman, J. M., Beese, L. S., Sanderson, M. R. & Steitz, T. A. (1988) *Proc. Natl. Acad. Sci. USA* **85,** 8924–8928.
8. Cowart, M., Gibson, K. J., Allen, D. J. & Benkovic, S. J. (1989) *Biochemistry* **28,** 1975–1983.
9. Beese, L. S., Derbyshire, V. & Steitz, T. A. (1993) *Science* **260,** 352–355.
10. Kuchta, R. D., Benkovic, P. & Benkovic, S. (1988) *Biochemistry* **27,** 6716–6725.
11. Carroll, S. S., Cowart, M. & Benkovic, S. J. (1991) *Biochemistry* **30,** 804–813.
12. Brenowitz, S., Kwack, S., Goodman, M. F., O'Donnell, M. & Echols, H. (1991) *J. Biol. Chem.* **266,** 7888–7892.
13. Guest, C. R., Hochstrasser, R. A., Dupuy, C. G., Allen, D. J., Benkovic, S. J. & Millar, D. P. (1991) *Biochemistry* **30,** 8759–8770.
14. Derbyshire, V., Grindley, N. D. F. & Joyce, C. M. (1991) *EMBO J.* **10,** 17–24.
15. Allen, D. J., Darke, P. L. & Benkovic, S. J. (1989) *Biochemistry* **28,** 4601–4607.
16. Allen, D. J. & Benkovic, S. J. (1989) *Biochemistry* **28,** 9586–9593.
17. Ludescher, R. D., Peting, L., Hudson, S. & Hudson, B. (1987) *Biophys. Chem.* **28,** 59–75.
18. Bevington, P. R. (1969) *Data Reduction and Error Analysis for the Physical Sciences* (McGraw–Hill, New York).
19. O'Connor, D. V. & Phillips, D. (1984) *Time-Correlated Single Photon Counting* (Academic, London).
20. Lai, M.-D. & Beattie, K. L. (1988) *Biochemistry* **27,** 1722–1728.
21. Brutlag, D. & Kornberg, A. (1972) *J. Biol. Chem.* **247,** 241–248.
22. Fersht, A. R., Knill-Jones, J. W. & Twui, W. C. (1982) *J. Mol. Biol.* **156,** 37–51.
23. Shatzsky-Schwartz, M., Hiller, Y., Reich, Z., Ghirlando, R., Weinberger, S. & Minsky, A. (1992) *Biochemistry* **31,** 2339–2346.
24. Joyce, C. M., Chen Sun, X. & Grindley, N. D. F. (1992) *J. Biol. Chem.* **34,** 24485–24500.
25. Petruska, J., Goodman, M. F., Boosalis, M. S., Sowers, L. C., Cheong, C. & Tinoco, I. T. (1988) *Proc. Natl. Acad. Sci. USA* **85,** 6252–6256.
26. Weiss, S. J. & Fisher, P. A. (1992) *J. Biol. Chem.* **267,** 18520–18526.
27. Maldonado-Rodriguez, R. & Beattie, K. L. (1991) *Mutat. Res.* **247,** 5–18.